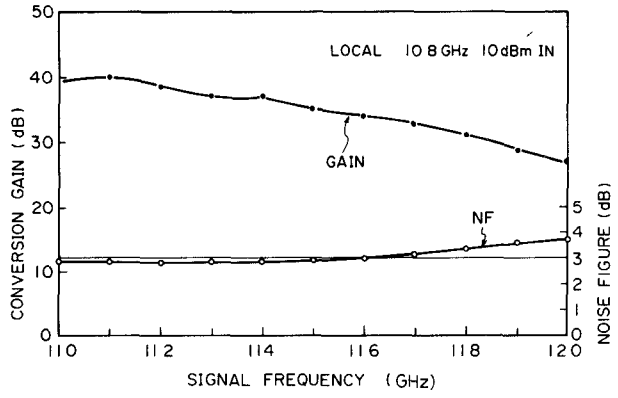

Fig. 10. Measured conversion gain and noise figure of the GaAs fully-monolithic frequency converter.

noise figure from the 11.3–12.2-GHz range. The figure also shows calculated conversion gain, which is in comparatively good agreement with the measured results. VSWR at the mixer RF input port was measured, supplying 8-dBm local oscillator power to the local oscillator signal input port. The VSWR was less than 3 over the 11.3–12.2-GHz range. The VSWR didn't depend strongly on the local oscillator power level.

Insertion loss for the filter is shown in Fig. 9. Maximum insertion loss is 15-dB at 8.7 GHz. Measured center frequency for the image rejection is lower than the designed frequency (9.65 GHz). Insertion loss for the RF band is approximately 1 dB. Measured relative bandwidth for more than 10-dB insertion loss for the double-tuning filter was about 40-percent superior to that for the single-tuning filter. Measured VSWR in the RF signal band was less than 2.5.

Since VSWR values for the amplifier, the filter, and the mixer is less than 3, appropriate total performances for the frequency converter chip can be expected.

Fig. 10 shows the experimental results for total conversion gain and noise figure on the GaAs fully-monolithic frequency converter. As shown in the figure, the frequency converter provides more than 34-dB conversion gain and less than 3.0-dB noise figure from 11.0–11.6 GHz. Saturation power output for the frequency converter was 7 dBm. DC power dissipation was 225 mW.

Since the frequency band and noise figure for the frequency converter are mainly determined by the amplifier characteristics, the frequency band for the frequency converter can be modified, mainly by changing the amplifier band.

V. Conclusion

Design considerations and microwave performances for the newly developed *X*-band GaAs monolithic frequency converter have been described. Multicircuit functions such as amplification, filtering, and mixing were integrated onto a single GaAs chip. The frequency converter provided more than 34-dB conversion gain and less than 3-dB noise figure in the 11.0–11.6-GHz range.

It has been demonstrated that reasonable performance can be obtained from a one-chip construction, MMIC-frequency converter, in which multicircuit functions were integrated. After proper modification based on the results, the frequency converter will be used in *X*-band systems, such as direct broadcast satellite reception, radar, or microwave communication systems.

Acknowledgment

The authors would like to thank T. Ozawa for ion implantation. They also would like to thank Y. Takayama and K. Kohzu for their constant encouragement throughout this work.

References

[1] T. Sugiura, H. Itoh, T. Tsuji, and K. Honjo, "12-GHz-band low-noise GaAs monolithic amplifiers" *IEEE Trans. Microwave Theory Tech.*, Vol. MTT-31, pp. 1083–1088, Dec. 1983.

[2] T. Sugiura, K. Honjo, and T. Tsuji, "12 GHz-band GaAs dual-gate MESFET monolithic mixer," in *1983 IEEE GaAs IC Symp Dig.*, Oct. 1983, pp. 3–6.

[3] C. Kermarrec, P. Harrop, C. Tsironis, and J. Faguet, "Monolithic circuits for 12 GHz direct broadcasting satellite reception," in *Microwave and Millimeter Wave Monolithic Circuit Symp. Dig.*, June 1982, pp. 5–10.

[4] S. Hori, K. Kamei, K. Shibata, M. Tatematsu, K. Mishima, and S. Okano, "GaAs monolithic MIC's for direct broadcast satellite receivers," *IEEE Trans. Microwave Theory Tech.*, vol. MTT-31, pp. 1083–1088, Dec. 1983.

[5] P. Harrop, P Lesarte, and A. Collet, "GaAs integrated all-front-end at 12 GHz," in *1980 GaAs IC Symp. Res. Abstracts*, paper no. 28.

[6] R A. Pucel, D. Masse, and R. Bera, "Performance of GaAs MESFET mixers at *X*-band," *IEEE Trans. Microwave Theory Tech.*, vol. MTT-24, pp. 351–360, June 1976.

[7] K Honjo, T Sugiura, T Tsuji, and T. Ozawa, "Low-noise low-power-dissipation GaAs monolithic broad-band amplifiers," *IEEE Trans. Microwave Theory Tech.*, vol. MTT-31, pp 412–417, May 1983.

[8] T Furutsuka, T. Tsuji, F. Katano, A. Higashisaka, and K Kurumada, "Ion-implanted E/D type GaAs IC technology," *Electron. Lett.*, vol. 17, no. 25/26, pp. 944–945, Dec. 1981.

A Novel Rectangular Waveguide with Double T-Septums

GOPA GUHA MAZUMDER AND PRADIP KUMAR SAHA

***Abstract*—A new rectangular waveguide with two T-shaped septums in place of solid rectangular ridges has been analyzed theoretically by the Ritz–Galerkin technique and is found to have superior cutoff and bandwidth characteristics of the dominant TE_{10} mode compared to the conventional ridged guides. Numerical data are presented and compared with those of symmetric double-ridged guides with identical gap parameters.**

I. Introduction

The ridges in rectangular waveguides are well known for their ability to increase both the cutoff wavelength and bandwidth of the dominant mode [1],[2]. The ridge dimensions can be optimized separately for the cutoff and bandwidth. Further improvements in these features are possible with dielectric filling of the ridge gap [3].

We propose a novel rectangular waveguide structure that is capable of significant improvement over the conventional ridged waveguide in respect of the cutoff wavelength and bandwidth of the dominant mode, even without any dielectric loading. The ridges are now made T-shaped instead of solid rectangular blocks as shown in Fig. 1. The structure remains homogeneous and should be much lighter as well.

Determination of the complete eigenvalue spectrum is not our aim at this time. It is known that for typical values of about 0.5 of the waveguide aspect ratio b/a, the dominant and the first higher order modes are TE_{10} and TE_{20}, respectively, in a conven-

Manuscript received January 10, 1985; revised June 24, 1985

The authors are with the Institute of Radio Physics and Electronics, 92 Acharya Prafulla Chandra Rd., Calcutta-700009, India.

0018-9480/85/1100-1235$01.00 ©1985 IEEE

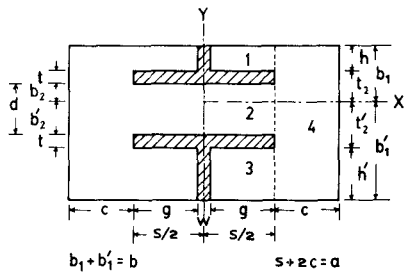

Fig. 1. Rectangular waveguide with two T-shaped septums.

tional ridged guide. This, however, can be ensured in any case by using suitable mode filters [3]. So, to study the cutoff and bandwidth characteristics of the new structure theoretically, we have analyzed it for the TE modes only using the Ritz–Galerkin technique [4].

The variation of the cutoff wavelength and bandwidth of the dominant mode of the new waveguide with the T-septum parameters are presented here and compared with those of the conventional double-ridged guide with identical ridge-gap dimensions.

II. Double T-Septum Guide (DTSG)

The structure shown in Fig. 1 is symmetric about the Y-axis, but an asymmetric gap location ($h \neq h'$) has been considered. This reduces to the conventional double-ridged guide (DRG) when, with d fixed, $s = w$ or $h = h' = 0$.

III. Analysis

Recently, in an analysis of the rectangular waveguides with two double ridges [5], [6], the Ritz–Galerkin technique was applied to the longitudinal apertures cascaded in the transverse direction. In the present case, we have multiple apertures in the same longitudinal plane which is treated by a variation of the same technique.

The formulation of the problem involves derivation of the integral equations for the unknown transverse electric fields over the apertures at $x = s/2$. These fields as functions of y are denoted by

$$\begin{aligned} &\text{(i)} && \xi_1(y), && t_2 \leqslant y \leqslant b_1 \\ &\text{(ii)} && \xi_2(y), && -b_2' \leqslant y \leqslant b_2 \\ &\text{(iii)} && \xi_3(y), && -b_1' \leqslant y \leqslant -t_2'. \end{aligned}$$

Two different symmetry cases of the magnetic and electric planes at $x = 0$ are considered simultaneously.

Firstly, the y-components of the electric fields and the z-components of the magnetic fields are matched at the apertures at $x = s/2$, and the amplitude coefficients of the field expansions in different regions are eliminated by expressing those in terms of ξ_1, ξ_2, and ξ_3. In the elimination, use is made of the fact that the E_y in region 4 vanishes over the edges of the septums. These manipulations result in the following integral equations:

$$F(y) = \sum_{m=0}^{\infty} \frac{\cot k_{x1m} g}{\epsilon_m h k_{x1m}} \cdot \cos \frac{m\pi}{h}(y - t_2) \cdot \int_{t_2}^{b_1} \xi_1(y') \cos \frac{m\pi}{h}(y' - t_2)\, dy', \qquad (t_2 \leqslant y \leqslant b_1) \quad (1)$$

$$F(y) = \sum_{n=0}^{\infty} (\epsilon_n d k_{x2n})^{-1} \left\{ \begin{matrix} -\tan \\ \cot \end{matrix} k_{x2n} s/2 \right\} \cdot \cos \frac{n\pi}{d}(y - b_2) \cdot \int_{-b_2'}^{b_2} \xi_2(y') \cos \frac{n\pi}{d}(y' - b_2)\, dy', \qquad (-b_2' \leqslant y \leqslant b_2) \quad (2)$$

$$F(y) = \sum_{l=0}^{\infty} \frac{\cot k_{x3l} g}{\epsilon_l h' k_{x3l}} \cdot \cos \frac{l\pi}{h'}(y + t_2') \cdot \int_{-b_1'}^{-t_2'} \xi_3(y') \cos \frac{l\pi}{h'}(y' + t_2')\, dy', \qquad (-b_1' \leqslant y \leqslant -t_2') \quad (3)$$

$$\epsilon_n = \begin{cases} 1, & n = 0 \\ 1/2, & n \neq 0 \end{cases}. \quad (4)$$

If k_c denotes the cutoff wavenumber, the transverse wave numbers in different regions are related to k_c through

$$k_c^2 = k_{x1m}^2 + (m\pi/h)^2 = k_{x2m}^2 + (m\pi/d)^2 = k_{x3m}^2 + (m\pi/h')^2 = k_{x4m}^2 + (m\pi/b)^2, \qquad m = 0,1,\cdots. \quad (5)$$

The upper and lower trigonometric functions in (2) correspond to magnetic and electric symmetry at $x = 0$, respectively. $F(y)$ on the left-hand side is defined as

$$F(y) = -\sum_{j=0}^{\infty} \frac{\cot k_{x4j} c}{\epsilon_j b k_{x4j}} \cos \frac{j\pi}{b}(y - b_1)\left[f_{1j} + f_{2j} + f_{3j}\right] \quad (6)$$

where

$$f_{1j} = \int_{t_2}^{b_1} \xi_1(y') \cos \frac{j\pi}{b}(y' - b_1)\, dy' \quad (7)$$

$$f_{2j} = \int_{-b_2'}^{b_2} \xi_2(y') \cos \frac{j\pi}{b}(y' - b_1)\, dy' \quad (8)$$

$$f_{3j} = \int_{-b_1'}^{-t_2'} \xi_3(y') \cos \frac{j\pi}{b}(y' - b_1)\, dy'. \quad (9)$$

To solve the integral equations by the Galerkin method, the following expansions of the aperture fields are substituted in (1)–(3):

$$\xi_1(y) = \sum_{i=0}^{M} A_{1i} \cos \frac{i\pi}{h}(y - t_2) \quad (10)$$

$$\xi_2(y) = \sum_{i=0}^{N} A_{2i} \cos \frac{i\pi}{d}(y - b_2) \quad (11)$$

$$\xi_3(y) = \sum_{i=0}^{L} A_{3i} \cos \frac{i\pi}{h'}(y + t_2'). \quad (12)$$

Inner products of (1)–(3) are then taken with $\cos[(q\pi/h)(y - t_2)]$, $q = 0,1,\cdots,M$, $\cos[(q\pi/d)(y - b_2)]$, $q = 0,1,\cdots,N$, and $\cos[(q\pi/h')(y + t_2')]$, $q = 0,1,\cdots,L$, respectively. This yields the following set of homogeneous equations:

$$\sum_{m=0}^{M} A_{1m} \left\{ \sum_{j=0}^{\infty} T_j X_{1qj} X_{1mj} + \delta_{qm} \epsilon_q h \frac{\cot k_{x1q} g}{k_{x1q}} \right\} + \sum_{n=0}^{N} A_{2n} \left\{ \sum_{j=0}^{\infty} T_j X_{1qj} X_{2nj} \right\} + \sum_{l=0}^{L} A_{3l} \left\{ \sum_{j=0}^{\infty} T_j X_{1qj} X_{3lj} \right\} = 0, \qquad (q = 0,1,\cdots,M) \quad (13)$$

TABLE I
VARIATION OF TE_{10} EIGENVALUE WITH NUMBERS OF FIELD EXPANSION TERMS

N	M = L	J	k_{c10} a (radians) s/a = 0.3	s/a = 0.9
1	1	1	1.2067	0.74996
1	5	5	1.1483	0.72913
1	10	10	1.1144	0.71760
5	5	5	1.1484	0.72918
5	10	10	1.1159	0.71817
5	10	30	1.1114	0.71700
10	5	10	1.1145	0.71763
10	10	20	1.1127	0.71729
10	15	30	1.1118	0.71716
15	5	10	1.1145	0.73670
15	10	20	1.1127	0.71729
15	15	30	1.1118	0.71715

WAVEGUIDE PARAMETERS: $b/a = 0.5$, $t/b = 0.05$, $d/b = w/a = 0.1$.

$$\sum_{m=0}^{M} A_{1m}\left\{\sum_{j=0}^{\infty} T_j X_{2qj} X_{1mj}\right\} + \sum_{n=0}^{N} A_{2n}\left\{\sum_{j=0}^{\infty} T_j X_{2qj} X_{2nj} + \delta_{qn}\epsilon_q d k_{x2n}^{-1}\begin{bmatrix}-\tan\\ \cot\end{bmatrix} k_{x2n} s/2\right\} + \sum_{l=0}^{L} A_{3l}\left\{\sum_{j=0}^{\infty} T_j X_{2qj} X_{3lj}\right\} = 0, \qquad (q = 0,1,\cdots,N) \tag{14}$$

$$\sum_{m=0}^{M} A_{1m}\left\{\sum_{j=0}^{\infty} T_j X_{3qj} X_{1mj}\right\} + \sum_{n=0}^{N} A_{2n}\left\{\sum_{j=0}^{\infty} T_j X_{3qj} X_{2nj}\right\} + \sum_{l=0}^{L} A_{3l}\left\{\sum_{j=0}^{\infty} T_j X_{3qj} X_{3lj} + \delta_{ql}\epsilon_q h' \frac{\cot k_{x3l} g}{k_{x3l}}\right\} = 0, \qquad (q = 0,1,\cdots,L) \tag{15}$$

$$X_{1lj} = \int_{t_2}^{b_1} \cos\frac{i\pi}{h}(y - t_2)\cos\frac{j\pi}{b}(y - b_1)\, dy \tag{16}$$

$$X_{2lj} = \int_{-b_2'}^{b_2} \cos\frac{i\pi}{d}(y - b_2)\cos\frac{j\pi}{b}(y - b_1)\, dy \tag{17}$$

$$X_{3lj} = \int_{-b_1'}^{-t_2'} \cos\frac{i\pi}{h'}(y + t_2')\cos\frac{j\pi}{b}(y - b_1)\, dy \tag{18}$$

$$\delta_{qm} = \begin{cases}1, & q = m\\ 0, & q \neq m\end{cases} \tag{19}$$

$$T_j = \frac{\cot k_{x4j} c}{\epsilon_j b k_{x4j}}. \tag{20}$$

The TE eigenvalue equation is obtained by setting to zero the determinant of the coefficient matrix of (13)–(15) for nontrivial solutions of A_{1i}, A_{2i}, and A_{3i}.

IV. NUMERICAL RESULTS

For numerical computation, only the doubly symmetric structures with $h = h'$ were considered. The j-summations were truncated after $J+1$ terms, that is, $J+1$ modes are taken into account in the expansion of the field in region 4. The variation of the normalized eigenvalue $k_c a$ of the dominant TE mode with the numbers of field expansion terms N, M, L, J is illustrated in Table I. The convergence is the first confirmation of the correctness of the analysis. All the subsequent computations were carried out with $N = M = L = 10$ and $J = 20$.

Another verification was obtained by computing the λ_c/a of the lowest TE mode for two cases of the septum dimensions approaching those of a solid ridge. For both the cases, the chosen gap parameters were $d/b = 0.1$ and $s/a = 0.5$. A conventional DRG with these parameters has $\lambda_c/a = 5.4$ for the dominant TE_{10} mode [7]. In the first case, with $w/a = 0$, t/b was varied from 0 to 0.45. In the second case, with $t/b = 0$, w/a was varied from 0 to 0.5. In both cases, the calculated values of λ_c/a of the lowest TE mode decreased continuously from 7.28 to 5.4.

The modal nomenclature of Montgomery [4] for ridged waveguides is adopted here for the DTSG. TE_{m0} hybrid modes are Y-polarized and are the basic ridged-waveguide modes of propagation. The trough modes are cross-polarized to the hybrid modes. To evaluate the useful TE_{10} hybrid–TE_{20} hybrid bandwidth of the structure, it must be determined whether the lowest root with electric symmetry along the Y-axis corresponds to the TE_{20} hybrid or TE_{10} trough mode. In a conventional ridged guide, the TE_{10} trough modes with electric and magnetic symmetry along the Y-axis may have almost coincident cutoff, particularly for narrow gaps, and may precede the TE_{20} hybrid cutoff in the mode spectrum [4]. An exactly similar spectrum was observed with the DTSG. For identifying the trough modes and locating the TE_{20} hybrid mode correctly from the roots of the eigenvalue equation, a separate computer program was set up for symmetry planes along both the Y- and X-axes.

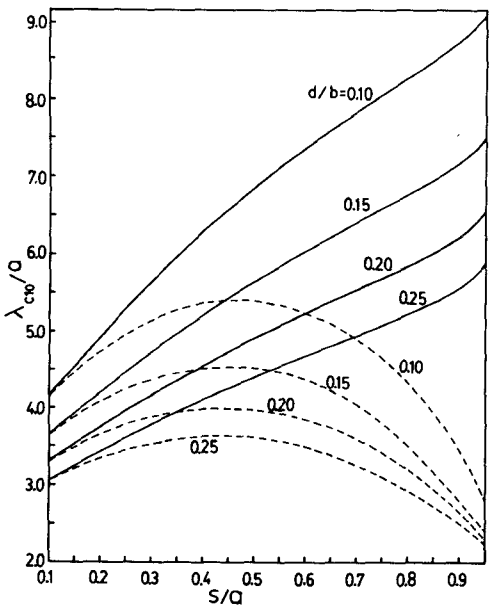

Fig. 2. Variation of normalized cutoff wavelength ($\lambda c_{10}/a$) of dominant TE_{10} mode with gap width ratio (s/a). $b/a = 0.50$. ———: DTSG ($t/b = 0.05$, $w/a = 0.10$). -------: DRG.

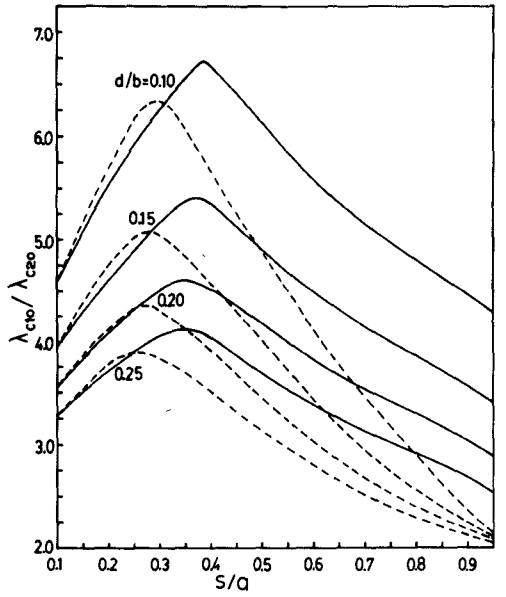

Fig. 3. Bandwidth characteristics. $b/a = 0.50$. ———: DTSG ($t/b = 0.05$, $w/a = 0.10$). -------: DRG

The normalized cutoff wavelength $\lambda c_{10}/a$ of the dominant TE_{10} hybrid mode as a function of the septum parameters is shown in Fig. 2. Also superposed is the $\lambda c_{10}/a$ of the symmetrical DRG [7] with identical d/b and s/a, subject to the usual error in reproducing from a graph. Not only are appreciably higher values of $\lambda c_{10}/a$ available, for a fixed d/b, but the cutoff wavelength increases monotonically with s/a. On the other hand, for a fixed s/a, $\lambda c_{10}/a$ decreases with increasing d/b. Although the data for fixed values of d/b up to 0.25 are presented, the nature of variation of $\lambda c_{10}/a$ with s/a remains the same for higher values of d/b. The curves were generated for $t/b = 0.05$ and $w/a = 0.1$. Slightly higher values of $\lambda c_{10}/a$ are obtained for still smaller values of these parameters. However, instead of computing for hypothetical zero values of these parameters, these have been given values very small but not unpractical.

The bandwidth characteristics of the new DTSG as well as the conventional DRG [7] are shown by the ($\lambda c_{10}/\lambda c_{20}$) versus ($s/a$) curves in Fig. 3, where λc_{20} is the cutoff wavelength of the TE_{20} hybrid mode. The two characteristics are very similar. The peaks of the curves for the DTSG are slightly higher and shifted toward higher values of s/a. However, beyond the peaks, the bandwidth of the DTSG falls less rapidly with s/a and remains substantially higher than that of the DRG.

V. Discussions

A novel broad-band rectangular waveguide with two T-shaped septums has been proposed as a better alternative to the conventional double-ridged guide. Structurally, such guides should be much lighter. Theoretical analysis reveals that for a fixed gap width ratio d/b, the cutoff wavelength of the dominant TE_{10} mode of these guides increases with the septum width ratio s/a and is much larger than that of the conventional ridged guides with wide ridges. The new guide also has considerably higher TE_{10}–TE_{20} mode separation for the values of s/a exceeding 0.3. Thus, in respect of the cutoff wavelength and bandwidth of the dominant TE_{10} mode, the proposed septum guide should offer much improved characteristics.

From the characteristics of a DRG, it may be concluded that its performance should not be very sensitive to small variations in the ridge dimensions when optimized for cutoff wavelength or bandwidth. For a DTSG, however, some tolerance on s/a should be imposed when the septum is to be designed for a large value of $\lambda c_{10}/a$. This can be relaxed if s/a is optimized for bandwidth. Computations show that both the $\lambda c_{10}/a$ and $\lambda c_{10}/\lambda c_{20}$ decrease with increasing septum thickness ratios t/b and w/a. At $s/a = 0.5$ and $d/b = 0.1$, a 5-percent variation in t/b (or w/a) at t/b (or w/a) = 0.1 produces a 0.25 percent change in both the $\lambda c_{10}/a$ and $\lambda c_{10}/\lambda c_{20}$.

Acknowledgment

The authors appreciate the encouragement from Prof. B. R. Nag during this work.

References

[1] S. B. Cohn, "Properties of ridge wave guide," *Proc. IRE*, vol. 35, 783–788, Aug. 1947.
[2] S. Hopfer, "The design of ridged waveguides," *IRE Trans. Microwave Theory Tech.*, vol. MTT-3, pp. 20–29, Oct. 1955.
[3] G. Magerl, "Ridged waveguides with inhomogeneous dielectric slab loading," *IEEE Trans. Microwave Theory Tech.*, vol MTT-26, pp. 413–416, June 1978.
[4] J. P. Montgomery, "On the complete eigenvalue solution of ridged waveguide," *IEEE Trans. Microwave Theory Tech.*, vol. MTT-19, pp. 547–555, June 1971.
[5] D. Dasgupta and P. K. Saha, "Eigenvalue spectrum of rectangular waveguide with two symmetrically placed double ridges," *IEEE Trans. Microwave Theory Tech.*, vol. MTT-29, pp. 47–51, Jan. 1981.
[6] D. Dasgupta and P. K Saha, "Rectangular waveguide with two double ridges," *IEEE Trans. Microwave Theory Tech.*, vol. MTT-31, pp. 938–941, Nov. 1983.
[7] T. S. Saad, Ed., *Microwave Engineers' Handbook*, vol 1. Dedham, MA: Artech House, 1971, pp. 87–88.